Research in Astronomy and Astrophysics, 24:085008 (15pp), 2024 August https://doi.org/10.1088/1674-4527/ad484e

The Influence of Different Solar System Planetary Ephemerides on Pulsar Timing

Jian-Peng Dai[1,2], Wei Han[2,3,4], and Na Wang[1,2,3,4]
[1] School of Physical Science and Technology, Xinjiang University, Urumqi 830046, China
[2] Xinjiang Astronomical Observatory, Chinese Academy of Sciences, Urumqi 830011, China; hanwei@xao.ac.cn, na.wang@xao.ac.cn
[3] University of Chinese Academy of Sciences, Beijing 100049, China
[4] Xinjiang Key Laboratory of Radio Astrophysics, Urumqi 830011, China
Received 2024 March 18; revised 2024 April 17; accepted 2024 May 5; published 2024 July 25

Abstract

Pulsar timing offers a comprehensive avenue for exploring diverse topics in physics and astrophysics. High-precision solar system planetary ephemeris is crucial for pulsar timing as it provides the positions and velocities of solar system planets including the Earth. However, it is inevitable that inherent inconsistencies exist in these ephemerides. Differences between various ephemerides can significantly impact pulsar timing and parameter estimations. Currently, pulsar timing highly depends on the JPL DE ephemeris, for instance, the Pulsar Timing Array data analysis predominantly utilizes DE436. In this study, we examine inconsistencies across various ephemeris series, including JPL DE, EPM, and INPOP. Notably, discrepancies emerge particularly between the current ephemeris DE436 and the earliest released ephemeris DE200, as well as the most recent ephemerides, e.g., DE440, INPOP21A, and EPM2021. Further detailed analysis of the effects of ephemeris on geometric correction procedures for the conversion of measured topocentric times of arrival is presented in this study. Our researches reveal that variations in the Roemer delays across different ephemerides lead to distinct differences. The timing residuals and the fact that these discrepancies can be readily incorporated into the subsequent pulsar parameters, leading to inconsistent fitting estimates, suggest that the influence of errors in the ephemeris on the timing process might currently be underappreciated.

Key words: (stars:) pulsars: general – Planetary Systems – time – ephemerides

1. Introduction

High-precision solar system planetary ephemerides are extensively utilized in a variety of fields, including planetary orbit observations, gravitational law verification, and deep space navigation. Notable examples of such ephemerides include the Development Ephemeris (JPL DE) series developed by the Jet Propulsion Laboratory (JPL) in the United States (Folkner et al. 2014; Rhodes et al. 2019), the Ephemeris of Planets and the Moon (EPM) series developed by the Institute of Applied Astronomy of the Russian Academy of Sciences (Pitjeva 2006, 2009), and the Integration Number Observation of Paris (INPOP) series developed by the Paris Observatory in France (Viswanathan et al. 2018; Fienga et al. 2022).

The solar system planetary ephemerides are the basis of pulsar timing. Pulsar timing plays an important role in both theoretical research and practical applications, such as detecting nanohertz gravitational waves, constraining the mass of solar system objects (Caballero et al. 2018), autonomous navigation of pulsars (Gui et al. 2023), and developing a pulsar-based timescale (Hobbs et al. 2020). The accuracy of pulsar timing has benefited from these large telescopes and has improved significantly, and the timing residuals of millisecond pulsars in the Pulsar Timing Array (PTA) projects are mostly better than 1 μs (Ridolfi et al. 2021; Wang et al. 2023).

Pulsar timing is particularly sensitive to the planetary ephemeris. This is due to the fact that an ephemeris provides essential planetary information for the pulsar timing process, such as the mass, position, and velocity of the solar system planets (Han et al. 2019). Therefore, the differences and errors inherent in an ephemeris have a certain impact on pulsar timing, especially for high-precision timing (Lazio et al. 2018). The difference in Roemer delay caused by different ephemerides (DE200, DE405, DE421, and DE430) was greater than 1 ms (Deng & Jin 2022). Conversely, the PTA data were used to constrain the upper mass limits of unidentified asteroids in the solar system (Caballero 2018), and well as the masses of the major planets in the solar system were estimated by analyzing pulsar timing data (Champion et al. 2011), in addition to the influence of ephemeris error on pulsar timing being studied by disturbing different parameters of the LINIMOS ephemeris (Guo et al. 2019). Pulsar timing can be used to study the reference frame rotation ties between different series of ephemerides (Liu et al. 2023).

The above studies are important for us to better understand the relationship between planetary ephemeris and pulsar timing, while there are still some unresolved issues worthy of exploration related to ephemeris and pulsar timing, for example, the precision of EPM and INPOP has been matched with that of JPL DE (Hilton & Hohenkerk 2011). However, the reference ephemerides currently used for pulsar timing research are mainly limited to the JPL DE series. The recognition of the other two types of ephemerides (EPM, INPOP) in current pulsar timing studies is still insufficient. The potential implications of errors in a referenced ephemeris are not comprehensively understood. Furthermore, the impact of these errors on pulsar timing and their subsequent influence on parameter estimations remain ambiguous. It is worth considering whether the use of the EPM and INPOP ephemerides could enhance pulsar timing.

In this study, we briefly compare the differences between different versions of JPL DE,[5] EPM,[6] and INPOP[7] ephemerides. The key information on the three ephemerides is provided in Table 5. We explore the impact of ephemeris inconsistencies on related pulsar timing correction terms, timing residuals, and pulsar parameter estimates using the software TEMPO2,[8] and the Parkes Pulsar Timing Array (PPTA)[9] data set. Based on our results, we provide a tentative recommendation for the selection of an ephemeris for future pulsar timing procedures.

2. The Impact of Ephemeris on Pulsar Timing

Different planetary ephemerides are used for pulsar timing in different periods or occasions. To assess the impact of ephemerides on timing, we conducted a comparative analysis of their inconsistencies. Furthermore, in an effort to broaden the applicability of these ephemerides, we incorporated two additional ephemerides (EPM, INPOP) into our reference set for pulsar timing.

2.1. The Pulsar Timing Model

The measured topocentric Time of Arrivals (TOAs) are transformed into the Solar System Barycenter (SSB) by the following operation, known as a timing model (Edwards et al. 2006)

$$\Delta t = \Delta_C + \Delta_A + \Delta_{E\odot} + \Delta_{R\odot} + \Delta_{S\odot} - D/f^2 + \Delta_{VP} + \Delta_B, \quad (1)$$

where Δ_C denotes the clock corrections, Δ_A signifies the atmospheric propagation delay, $\Delta_{E\odot}$ represents the delay due to the solar system's Einstein correction, $\Delta_{R\odot}$ corresponds to the solar system's Roemer correction, $\Delta_{S\odot}$ is associated with the solar system's Shapiro correction, D/f^2 stands for the dispersion delay, while Δ_{VP} captures the Shklovskii effect induced by long-term proper motion and the delay resulting from the radial movement of pulsars. Additionally, Δ_B encompasses various delays arising from the orbital motion of binary pulsars.

Here we illustrate the following terms that are closely related to planetary ephemeris:

(1) Roemer delay:

$$\Delta_{R\odot} = -\frac{\vec{r}\cdot\hat{R}_{BB}}{c}, \quad (2)$$

where $\vec{r}$ denotes the position vector of the Earth in relation to the SSB, while $\hat{R}_{BB}$ signifies the direction vector from the observation station to the pulsar. This vector illustrates the geometric delay experienced by light propagation between the observation station and the SSB. It is the most significant time correction term, extending up to 500 s. Additionally,

$$\hat{R}_{BB} = \hat{R}_0 + \mu_\perp(t_a^{BB} - t_{pos}) - \tfrac{1}{2}(|\mu_\perp|^2\hat{R}_0 + \mu_\parallel\mu_\perp)(t_a^{BB} - t_{pos})^2, \quad (3)$$

$\hat{R}_0$ represents the direction vector from the SSB to the pulsar, whereas $\mu_\parallel$ and $\mu_\perp$ delineate the radial and lateral components of the proper motion, respectively.

(2) The Shapiro delay arises due to the gravitational influence of a massive celestial body on the path of light propagation, also referred to as the gravitational effect delay,

$$\Delta_{S\odot} = -2\sum\frac{GM_i}{c^3}\ln(\hat{R}_{BB}\cdot|\vec{r}_i|) + \Delta_{S\odot 2}, \quad (4)$$

where M_i and $\vec{r}_i$ represent the mass and position vector of the ith celestial body in relation to the SSB. The term $\Delta_{S\odot 2}$ represents the second-order correction. Within the solar system, the Sun and Jupiter exhibit the most pronounced Shapiro delay effect when compared to all other celestial bodies.

(3) The Einstein delay arises from relativistic time dilation and gravitational redshift, both of which are caused by the motion of the observing clock relative to the SSB. TEMPO2 obtained the delay from TE405, a numerical ephemeris of the Earth used for the conversion between TT and TCB based on DE405, with an error of less than 5 ns at the time (Irwin & Fukushima 1999). Since TE405 has not been updated, it is difficult to analyze the difference in Einstein delay in this study.

It is important to identify the magnitude of the correction terms with different ephemerides, based on which further analysis can be conducted. The typical sizes of the above

[5] The website for the JPL DE: https://ssd.jpl.nasa.gov/planets/eph export.html/.
[6] The website for the EPM: https://iaaras.ru/en/dept/ephemeris/epm/.
[7] The website for the INPOP: https://www.imcce.fr/recherche/equipes/asd/inpop/.
[8] The soft version is tempo2-2021.06.1, obtained from: https://bitbucket.org/psrsoft/tempo2/downloads/.
[9] The website for the PPTA data set: http://www.ipta4gw.org/.

Table 1
Typical Size of Partial Delay Items Included in TEMPO2 Program

Delay Item	Value/μs	Delay item	Value/μs
Einstein delay	1600	Shapiro delay due to Jupiter	0.180
Roemer delay	5E+8	Shapiro delay due to Saturn	0.058
Shapiro delay due to Sun	112	Shapiro delay due to Uranus	0.010
Shapiro delay due to Venus	0.0005	Shapiro delay due to Neptune	0.012

correction terms are presented by Edwards et al. (2006) and listed in Table 1.

2.2. Inconsistency in the Solar System Planetary Ephemeris

The planetary ephemeris, which is essentially tables or databases that contain timed information on the position and motion of celestial objects, plays a significant role in understanding the dynamics of our solar system.

Factors such as observational data, dynamic models, as well as the definitions of different reference frames and coordinate systems inevitably result in inconsistencies between various ephemerides. These differences are primarily manifested in the positional variances of large celestial bodies relative to the SSB. In terms of reference frame, DE421 and DE405 utilize International Celestial Reference Frame (ICRF) (Liu 2021), achieving an alignment accuracy of approximately 0.25 mas and 1 mas respectively. In contrast, DE430 employs International Celestial Reference Frame 2 (ICRF2) (Yao et al. 2022), which has achieved an alignment accuracy of 0.2 mas. The most recent versions, DE440, DE441, EPM2021, and INPOP21A, adopt International Celestial Reference Frame 3 (ICRF3) (Jiang et al. 2023), leading to further advancements in alignment precision.

For example, in earlier versions of DE405 and DE421, the positional differences between Earth and Jupiter relative to the SSB could be tens of meters and tens of kilometers, respectively (Deng et al. 2013). In DE421 and DE430, the positional differences between Earth, Mercury, Venus, and Mars relative to the SSB could be tens of kilometers, as well as the positional differences between Earth, Mercury, Venus, and Mars relative to the SSB reaching 100 km in DE430 and DE440 (Sun et al. 2022). Likewise, the relative distances between the Moon and the Earth in DE430 and INPOP19 are several tens of centimeters (Liu et al. 2022).

Furthermore, several ephemerides are specifically designed for distinct space missions. For instance, DE421 focuses on supporting and facilitating the coordinate transformation between the lunar center inertial system and the lunar fixed system in the Gravity Recovery and Interior Laboratory (GRAIL) mission (Lehman et al. 2013). The primary objective of this mission is to elucidate the internal structure of the Moon through highly precise gravity mapping. Given that the GRAIL mission encompasses data from two lunar probes (GRAIL A and GRAIL B), DE421 may not be optimally suited for pulsar timing.

Owing to the release time being too long, DE200 is largely obsolete in both current and future astrometry and pulsar timing practices. Consequently, the comparison of time correction terms, residuals, and pulsar parameters using DE200 as a reference may offer limited value for future pulsar timing endeavors. Accordingly, the comparison results of DE200 are not provided in our research.

2.3. The Position Difference of the Earth

The SSB does not align with the center of the Sun, instead, the Earth orbits the Sun, and the Sun in turn orbits the SSB, so the position vector of the Earth relative to the SSB can be decomposed as follows

$$\vec{r}_{\mathrm{earth\_ssb}} = \vec{r}_{\mathrm{earth\_}} + \vec{r}_{\mathrm{\_ssb}}, \tag{5}$$

where $\vec{r}_{\mathrm{earth\_}}$ denotes the position vector of the Earth in relation to the Sun's center, and $\vec{r}_{\mathrm{\_ssb}}$ signifies the position vector of the solar center relative to the SSB.

We explore the positional discrepancies of the Earth based on various ephemerides, and DE436 has been employed as the reference ephemeris in our work. We compare the discrepancies between the Earth's and the Sun's positions relative to the SSB with those derived from DE436. In Figure 1 we show the patterns of change between $\vec{r}_{\mathrm{earth\_}}$, $\vec{r}_{\mathrm{\_ssb}}$, and $\vec{r}_{\mathrm{earth\_ssb}}$. Meanwhile, Table 2 presents the statistical analysis of the absolute value of the X, Y, Z coordinate difference across various ephemerides, including maximum, average, and rms values.

The first column presents the variations in $\vec{r}_{\mathrm{earth\_}}$, which are approximately annual terms. These primarily stem from perturbations in the Earth's orbit, attributed to mass errors associated with the inner planets (Mercury, Venus, Mars, and Earth) (Guo et al. 2019). In addition, these differences generally diminish as the three series of ephemeris versions undergo updates.

The second column indicates the differences in $\vec{r}_{\mathrm{\_ssb}}$, which arise from alterations in the solar system's mass distribution, attributed to mass errors from larger planets (Jupiter, Saturn, Uranus, and Neptune), as well as other unidentified celestial bodies (Champion et al. 2011). Theoretically, given a sufficient

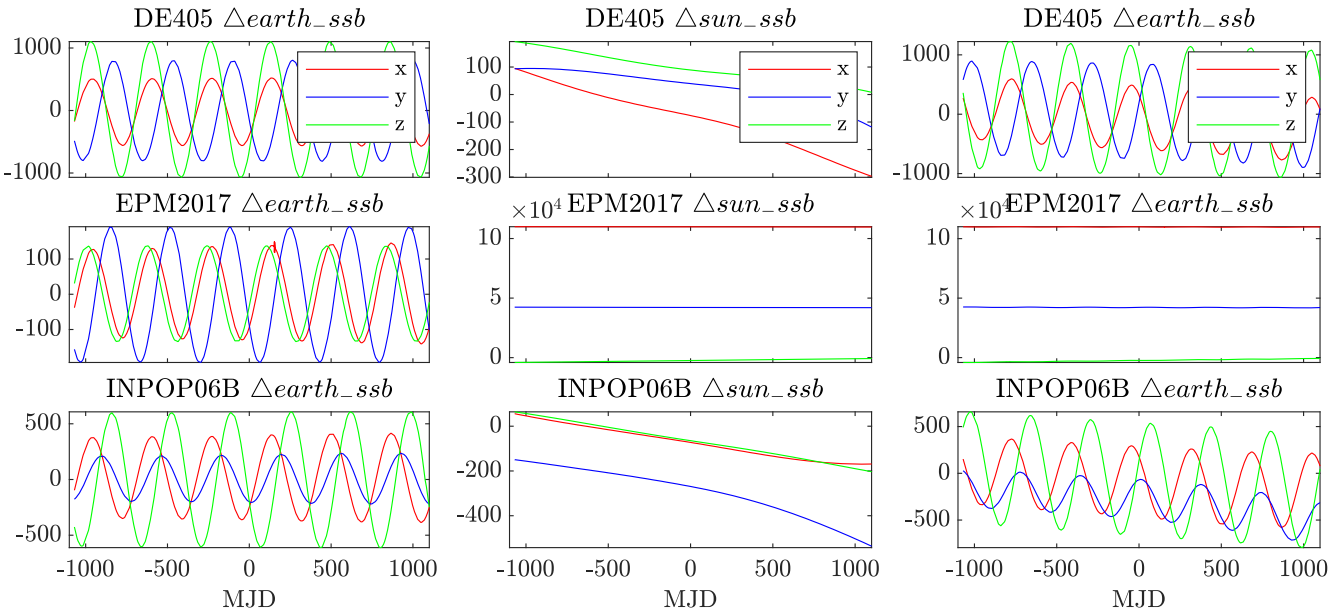

Figure 1. Position differences of $\vec{r}_{\text{earth\_}}$, $\vec{r}_{\text{\_ssb}}$, and $\vec{r}_{\text{earth\_ssb}}$ with different ephemerides. The plots, arranged from top to bottom, depict the positional discrepancies between a specific ephemeris and DE436. MJD0 is 54500 (2008 February 4), and the vertical coordinate is in meters.

Table 2
Max, Mean, and rms of the Earth Position Difference Relative to the SSB in 2005–2011.

Ephemeris	Statistic	X/m	Y/m	Z/m	R/m
DE436−DE405	Max	252.151	769.975	895.400	1223.933
	Mean	87.179	356.812	527.170	718.816
	rms	101.496	403.664	576.859	794.874
DE436−DE421	Max	197.623	192.403	377.742	219.573
	Mean	124.752	85.646	204.562	83.263
	rms	137.968	103.167	237.618	99.811
DE436−DE438	Max	29.226	33.638	38.652	74.348
	Mean	11.906	14.345	13.997	32.912
	rms	14.418	17.573	17.380	38.734
DE436−DE440	Max	115618.317	107748.057	47094.986	3017.886
	Mean	70618.151	107478.950	46982.328	1374.727
	rms	78635.211	107479.044	46982.359	1581.928
DE436−EPM2011	Max	110364.800	93150.528	60883.201	11795.948
	Mean	69436.062	92193.582	59944.329	10527.688
	rms	75860.763	92194.598	59945.612	10546.634
DE436−EPM2021	Max	127238.347	112931.813	64211.811	2641.791
	Mean	79114.692	112035.585	63900.701	1167.584
	rms	86974.755	112036.386	63900.818	1357.572
DE436−INPOP06B	Max	564.703	579.657	714.404	794.827
	Mean	202.810	256.087	279.286	374.514
	rms	239.123	295.804	325.108	420.565
DE436−INPOP08A	Max	438.626	968.372	981.132	445.838
	Mean	147.455	439.358	461.037	179.067
	rms	175.884	492.164	534.123	217.935
DE436−INPOP17A	Max	225.694	197.513	270.751	292.579
	Mean	127.600	88.903	143.599	114.643
	rms	140.836	110.087	155.365	143.595
DE436−INPOP21A	Max	43321.019	9111.830	46586.047	1977.030
	Mean	28742.924	8249.477	45702.115	656.046
	rms	31829.154	8260.409	45704.564	827.056

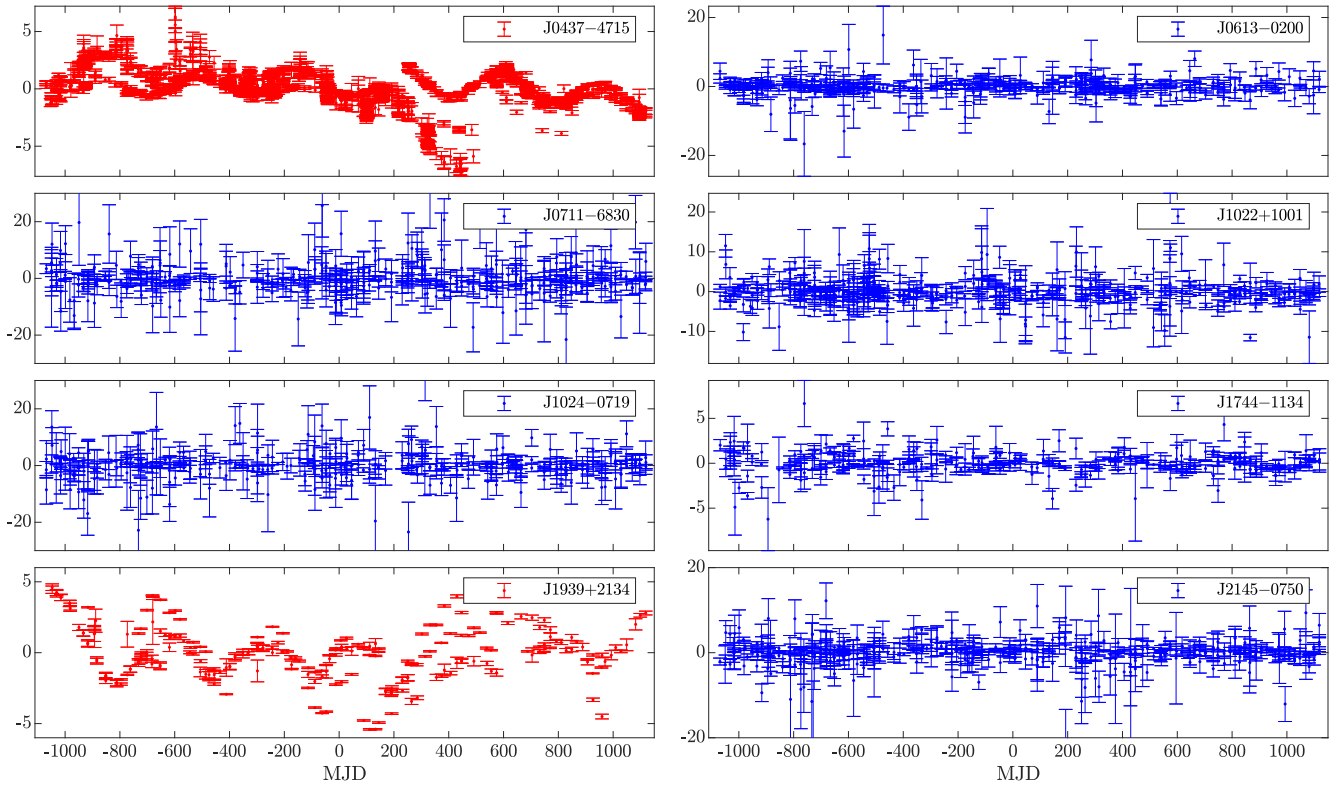

Figure 2. The residuals of each pulsar with the DE436. PSRs J0437−4715 and J1939+2134, exhibit structural noise, while the remaining pulsars present white noise. MJD0 is 54500, and the vertical axis represents the residual in microseconds.

Table 3
Some Basic Characteristics of Pulsars Involved in This Study

Pulsar	J0437−4715	J0613−0200	J0711−6830	J1022+1001
RAJ/hms	04:37:15.8147248(98)	06:13:43.9755451(54)	07:11:54.1891774(88)	10:22:58.0022994(63)
DEC/dms	−47:15:08.62249(2)	−02:00:47.21132(1)	−68:30:47.41440(8)	+10:01:52.83727(3)
F0/s^{-1}	173.687946184747(3)	326.600562067685(7)	182.117234668580(7)	60.779447963614(2)
F1/s^{-2}	−1.728275E-15	−1.022866E-15	−4.944286E-16	−1.600928E-16
NTOAs	2039	411	401	441
Binary	T2	T2	No	T2
rms/μs	0.212	1.068	0.858	1.560
Pulsar	J1024−0719	J1744−1134	J1939+2134	J2145−0750
RAJ/hms	10:24:38.6786394(44)	17:44:29.4058033(50)	19:39:38.5612552(53)	21:45:50.4614935(69)
DEC/dms	−07:19:19.36785(8)	−11:34:54.68123(6)	+21:34:59.12637(4)	−07:50:18.47573(5
F0 s^{-1}	193.715683478599(9)	245.426119713058(3)	641.928226453444(4)	62.2958878423848(7)
F1 s^{-2}	−6.957674E-16	−5.381295E-16	−4.330868E-14	−1.156083E-16
NTOAs	342	305	235	414
Binary	No	No	No	T2
rms/μs	1.470	0.367	1.660	0.877

data span, these differences should appear as periodic terms. However, they currently behave like long-term drifts, with significant discrepancies between different versions. It is worth noting that the differences with respect to DE440, EPM2021, and INPOP21A can reach up to an order of 10 km, due to the inclusion of over 30 newly discovered Kuiper Belt objects (KBOs) into the models of the three latest ephemerides (Park et al. 2021).

The final column represents the difference of $\vec{r}_{\rm earth\_ssb}$, which is the vector sum of the previous two columns. These

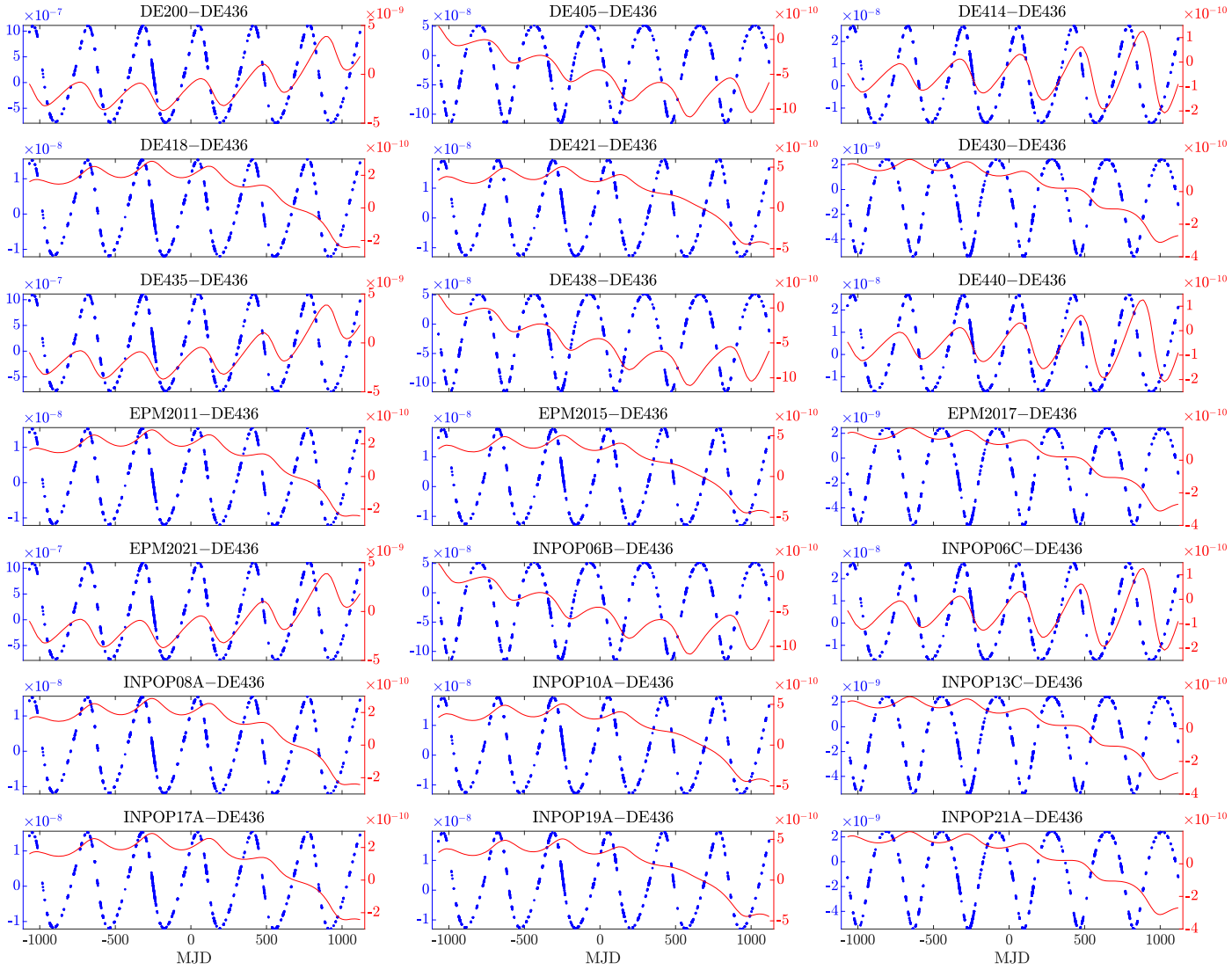

Figure 3. The differences of Shapiro delays for PSR J0437−4715 represented in milliseconds, in which each panel depicts the result corresponding to a specific ephemeris, with MJD0 set at 54500. The blue scatter and the red curve represent the Shapiro delays caused by Jupiter and the Sun respectively, and they have different scales on the left and right *Y*-axes.

differences are approximately superposed by the annual term and long-term drift. According to a pulsar timing model, these two types of positional differences can lead to the expected annual terms and long terms in the associated corrections, resulting in different timing residuals and pulsar parameter fitting results.

3. Pulsar Timing Analysis Based on the PPTA Data Set

3.1. The Data set and Software

The PPTA_DR2 data sets are utilized in our study. The PPTA is one of the most significant timing arrays in the world based on observations with the Parkes 64 m radio telescope, which dates back to early 2005. Its primary goals include the direct detection of gravitational waves (Vallisneri et al. 2020), the establishment of a pulsar-based timescale (Hobbs 2015), and the enhancement of planetary ephemeris (Li et al. 2016). The project has gathered 18 yr of observation data on dozens of pulsars. We use eight pulsars within the PPTA_DR2 for our investigation, including binary and single pulsars with different periods, residual levels, noise types, and positions. Figure 2 and Table 3 show the basic information about these pulsars derived from the TEMPO2 software.

The TEMPO2 software released in 2006 is widely used for pulsar timing and analysis. It calculates the barycentric TOAs, forms timing residuals, and carries out pulsar parameter fitting.

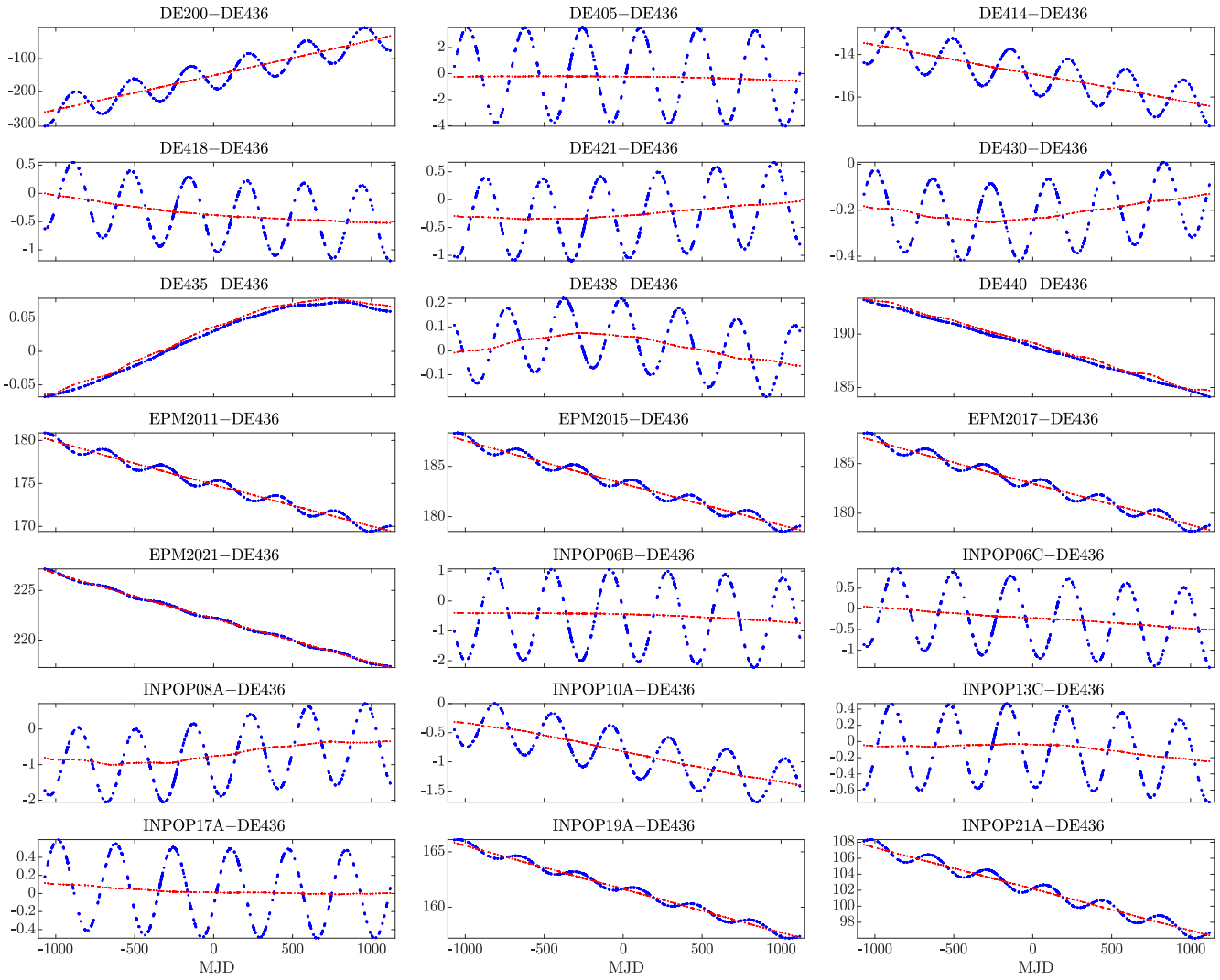

(a) Differences of Roemer delays for PSR J0437−4715

Figure 4. The differences of Roemer delays, in which each subgraph represents the result with a specific ephemeris. The blue curves depict the pre-fit Roemer delay differences, whereas the red curves are the variations post-fitting for positions and proper motions. MJD0 is 54500, and the vertical coordinate is in microseconds.

TEMPO2 is in accordance with the IAU2000 resolution, and utilizes the ICRS reference frame and the TCB time standard, taking into account all known interference factors beyond 1 ns (Edwards et al. 2006; Hobbs et al. 2006; Hobbs 2012).

We only employ the weighted least squares (WLS) approach in TEMPO2 for pulsar parameter estimation. Furthermore, TEMPO2 only supports the JPL DE series ephemeris by default, so we made necessary modifications to adapt the TEMPO2 program and ephemeris.

3.2. Analysis of Shapiro Delay Differences

The Shapiro delays of the Sun and major planets can be derived from TEMPO2. Discrepancies in Shapiro delays with different ephemerides can be identified by comparisons with those derived from DE436. We demonstrate the differences in Shapiro delay of the Sun and Jupiter for PSRs J0437−4715 and J0613−0200 in Figure 3, which show both annual terms and long-term drifts, with amplitudes less than 10^{-7} ms. Given the precision of current timing, these differences can be negligible. Other pulsars demonstrate similar results which are omitted here.

3.3. Analysis of Roemer Delay Differences

As per Equation (2), inconsistencies in the Earth's position due to different ephemerides can lead to inconsistencies in Roemer delays. This, in turn, influences both timing residuals and pulsar parameters. In order to have a clearer understanding

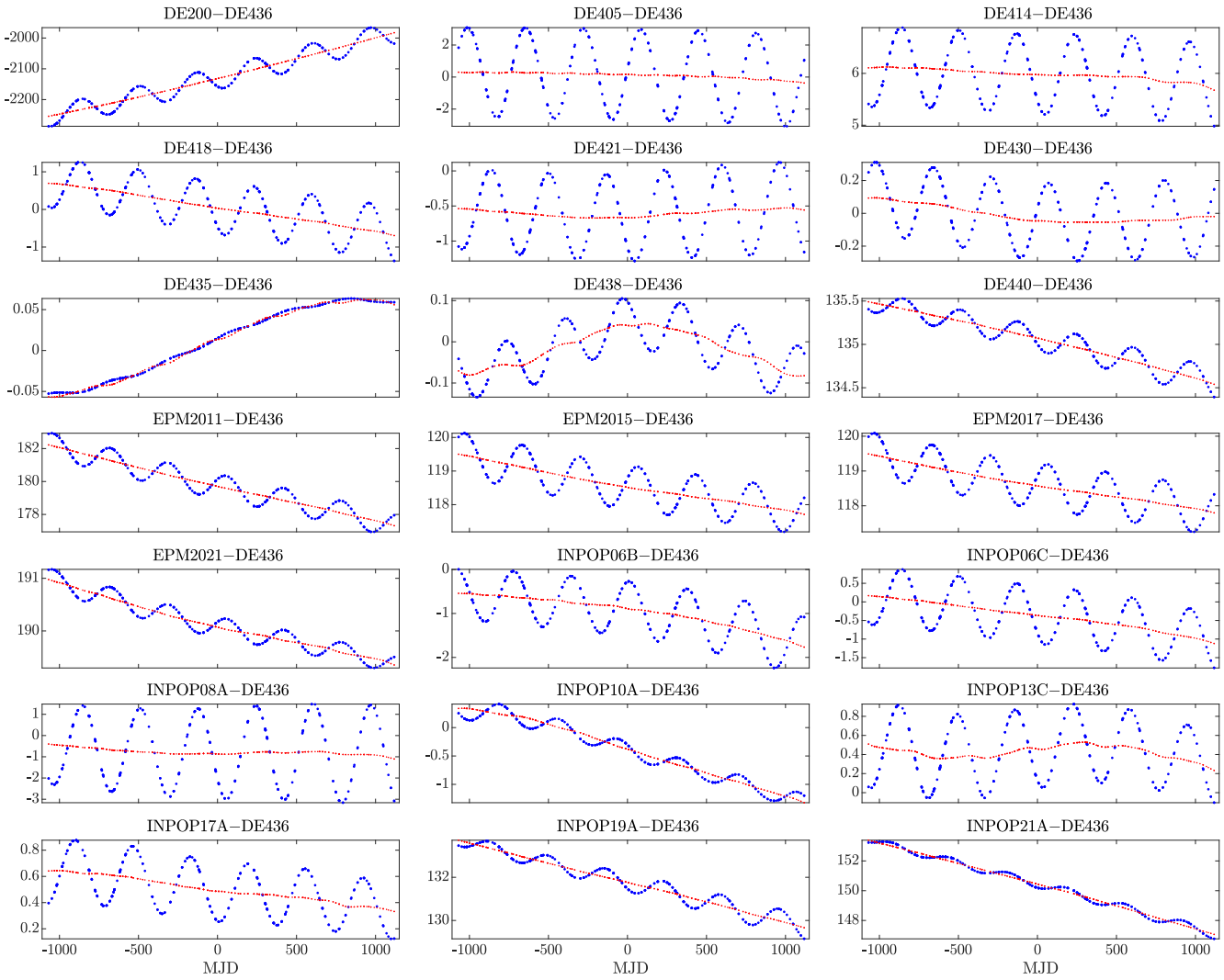

(b) Differences of Roemer delays for PSR J0613−0200

Figure 4. (Continued.)

of this effect, we calculate the pre-fit Roemer delay corrections with a given ephemeris, then recalculate the post-fit Roemer delay corrections after fitting RAC, DECJ, PMRA, and PMDEC. The differences of Roemer delay are obtained by comparing the pre-fit and post-fit Roemer delay with those obtained by DE436. Figure 4 shows the differences of the Roemer delays for PSRs J0437−4715 and J0613−0200. It can be seen that:

1. Before parameter fitting, there are annual terms and long-term drifts in the Roemer delay differences with different amplitudes and systematic biases, primarily attributable to the discrepancy of $\vec{r}_{\rm earth\_}$ and $\vec{r}_{\rm \_ssb}$ respectively. Notably, these differences are particularly pronounced for data derived from DE200, DE440, EPM2011, EPM2015, EPM2017, EPM2021, INPOP19A, and INPOP21A.
2. The long-term drifts of the Roemer delay difference show no clear change after the pulsar parameters are fitted. This suggests that the long-term drift does not influence the positional and proper motion parameters. Instead, these parameters predominantly absorb the annual terms, leaving only long-term drifts.

3.4. Analysis of Residual Differences

We also obtain differences between pre-fit and post-fit timing residuals after fitting for RAC, DECJ, F0, F1, PMRA,

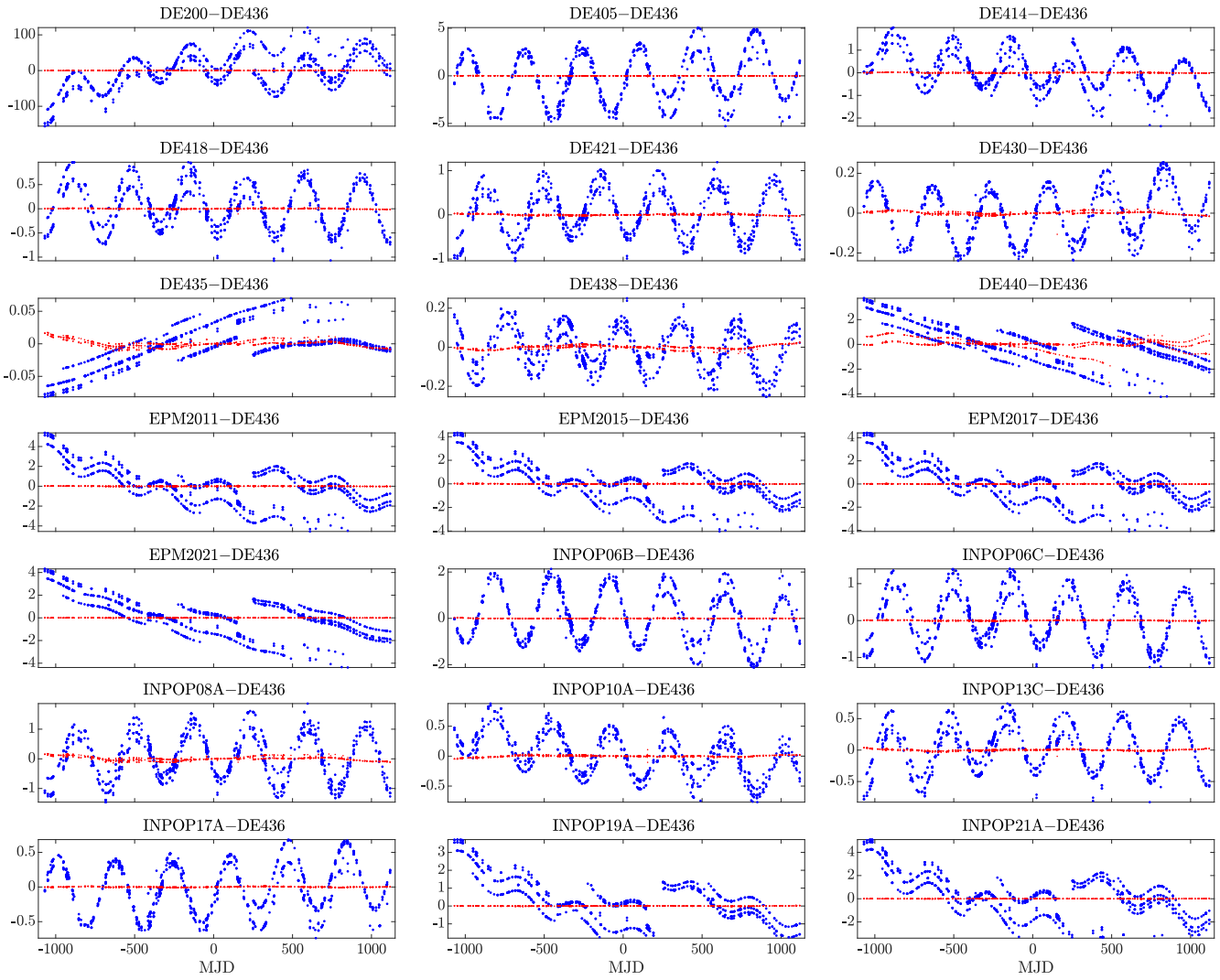

(a) Differences of residuals for PSR J0437−4715

Figure 5. The differences of residuals, in which each subgraph represents the result with a specific ephemeris. The blue curves depict the pre-fit residual differences, whereas the red curves are the variations post-fitting for positions, proper motions and rotations. MJD0 is 54500, and the vertical coordinate is in microseconds.

and PMDEC, which are shown in Figure 5. The rms values of the residual differences are shown in Figure 6.

Figure 5 shows that there are clear annual terms and long-term drifts in the timing residuals before fitting pulsar parameters. After fitting for the astrometric and rotational parameters, these patterns are significantly reduced, indicating that the two components of the Earth's position difference have independent effects on timing residuals. Furthermore, the influence of the ephemeris on pulsar timing is reflected in both timing residuals and pulsar parameter estimates. According to Figure 6, the rms values of the residual differences with different ephemerides show variations. This suggests that the impact of ephemeris on pulsar timing is universal.

3.5. Analysis of Pulsar Parameters

To assess the impact of various ephemerides on pulsar parameters, we fitted RAC, DECJ, F0, F1, PMRA, and PMDEC. Table 4 shows the fitted parameters of PSR J0437 −4715. Some parameters are only displayed with their decimal parts with difference for clarity, and their corresponding same part is given under the parameter name. We can find that:

1. The discrepancies could be larger than the uncertainties with different ephemerides, indicating that the ephemeris exerts a significant influence on pulsar parameters.
2. The results for positional and proper motion parameters exhibit significant differences when comparing the

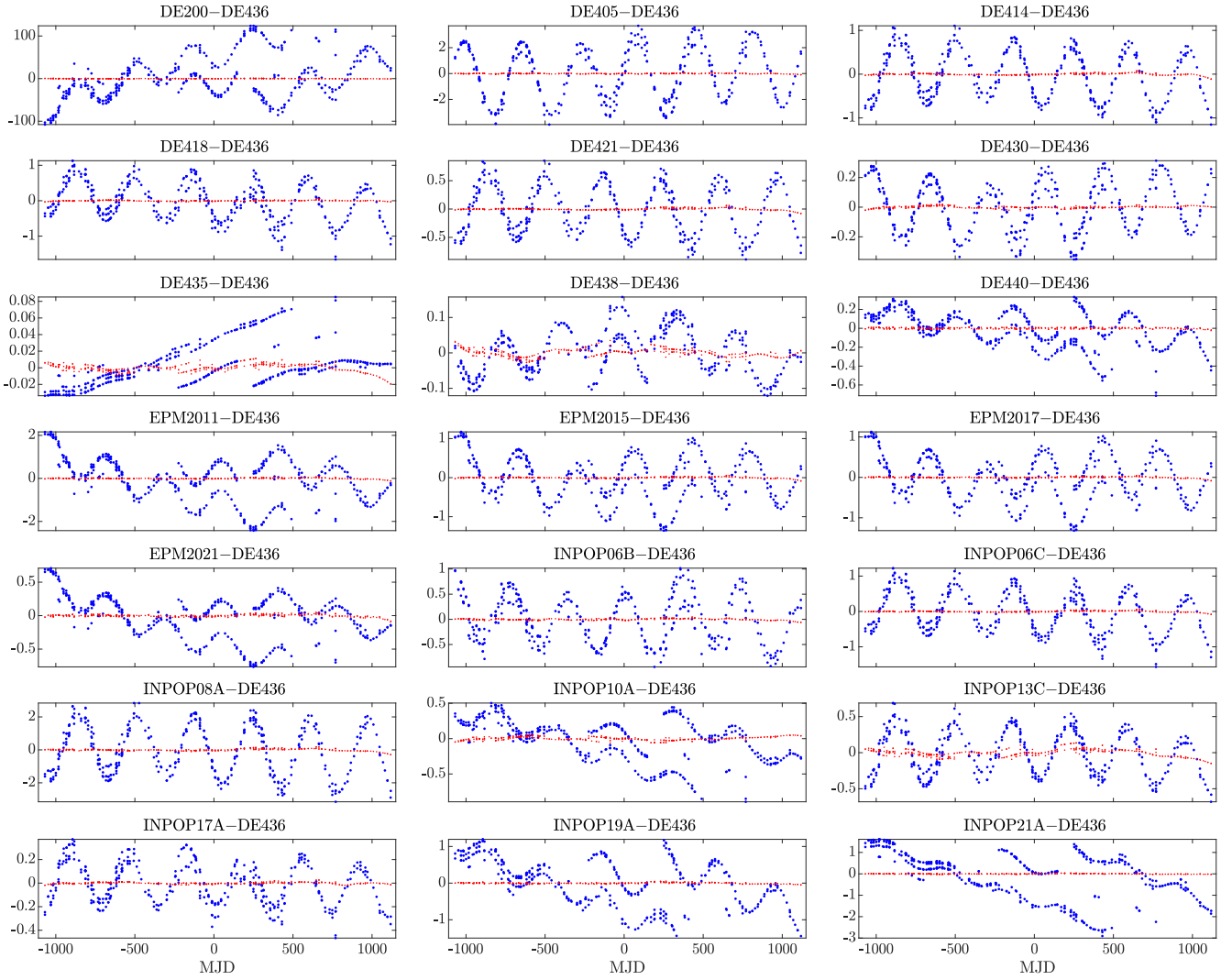

(b) Differences of residuals for PSR J0613−0200

Figure 5. (Continued.)

DE200 and DE405 with the DE436. Additionally, discrepancies are also present in the results associated with the DE414, DE418, DE421, EPM2011, EPM2015, EPM2017, INPOP06B, INPOP06C, and INPOP08A. Meanwhile, attention should be paid to discrepancies of F0 and F1 in high-precision timing and application.

4. Evaluation and Suggestion

The ephemeris errors can influence the delay terms and residuals, which in turn affects the estimation of pulsar parameters. Therefore, these parameters can be a good indicator of the overall performance of the ephemeris. We use the Rank Sum Ratio (RSR) method (Ao & He 2020) to assess the ephemeris as follows:

(1) We take 21 ephemerides as the evaluation objects, and then calculate the deviation of six parameters. The final parameter deviation matrix is shown as follows

$$P = \begin{bmatrix} \triangle RAJ_1 & \triangle DEC_1 & \triangle F0_1 & \triangle F1_1 & \triangle PMRA_1 & \triangle PMDEC_1 \\ \triangle RAJ_2 & \triangle DEC_2 & \triangle F0_2 & \triangle F1_2 & \triangle PMRA_2 & \triangle PMDEC_2 \\ & & & \ddots & & \\ \triangle RAJ_{21} & \triangle DEC_{21} & \triangle F0_{21} & \triangle F1_{21} & \triangle PMRA_{21} & \triangle PMDEC_{21} \end{bmatrix}, \quad (6)$$

for example, the RAJ deviation is expressed as: $\triangle \mathrm{RAJ}_i = |\mathrm{RAJ}_i - \mathrm{RAJ}_{DE436}|$.

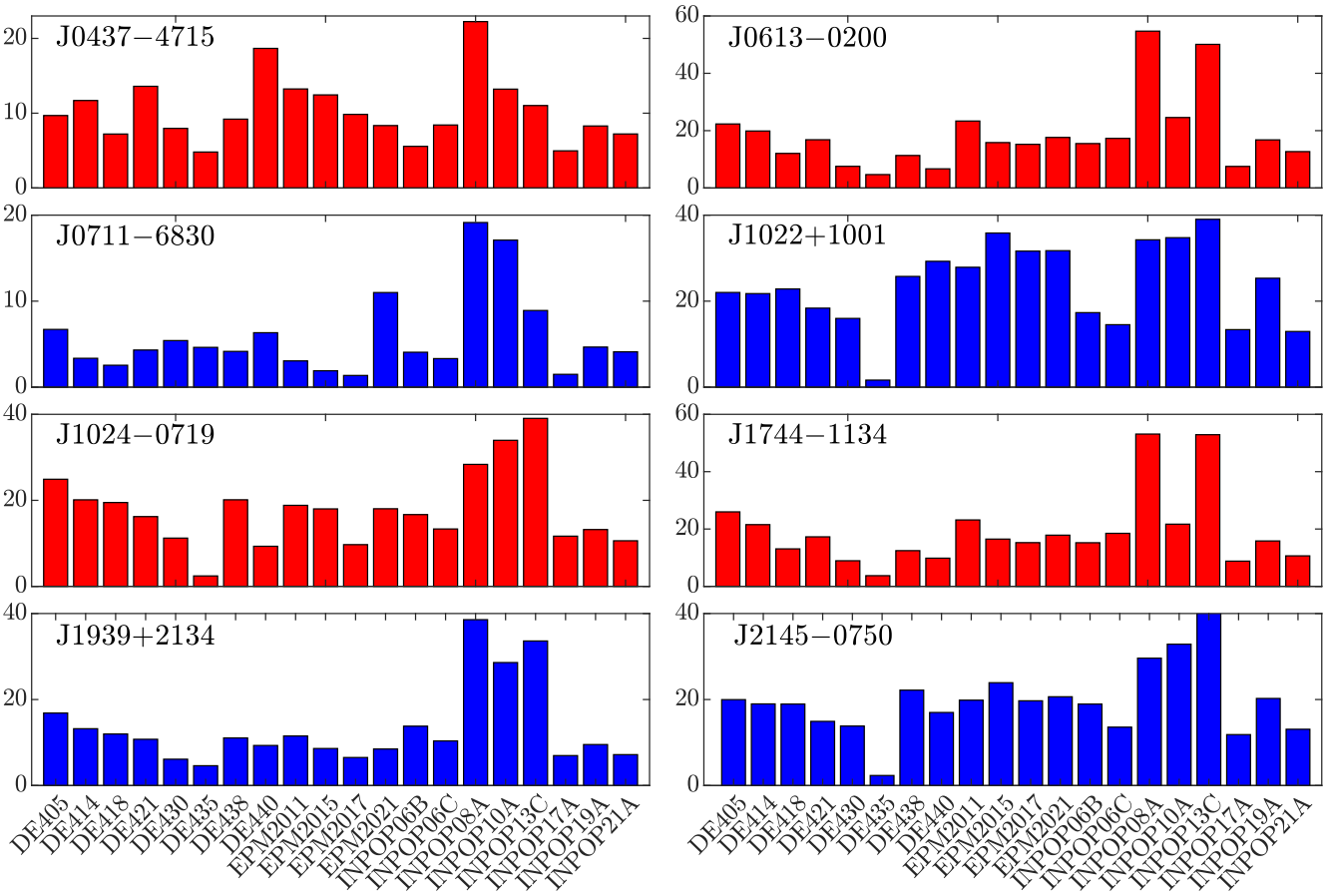

Figure 6. The rms of post-fit residual differences, in which each subgraph represents a pulsar, the abscissa is ephemeris version, and the vertical coordinate is measured in nanoseconds. It should be noted that the bar value is not the residual rms of each pulsar, rather, it represents the rms of the difference of residuals. For instance, the ordinate of DE405 signifies that the residual of DE405 is subtracted from the residual of DE436. The difference between these two at the corresponding MJD is then calculated, and its rms is derived.

(2) Sort each column of data in the matrix P in descending order (as the parameter difference is a low-quality indicator), using an element's order number as a rank. This process will yield the rank matrix R

$$R = \begin{bmatrix} R_{11} & R_{12} & \dots & R_{1n} \\ R_{21} & R_{22} & \dots & R_{2n} \\ & & \ddots & \\ R_{m1} & R_{m2} & \dots & R_{mn} \end{bmatrix}. \quad (7)$$

Similar to P, matrix R is composed of a 21×6 structure, in which 21 rows symbolize the 21 evaluation subjects or ephemerides, while the six columns represent the six evaluation indicators or parameters.

(3) We then calculate the RSR value of each ephemeris for a given pulsar

$$RSR_i = \sum_{j=1}^{n} \frac{R_{ij}}{m \times n}, \quad (8)$$

where R_{ij} represents the rank of the elements in matrix P situated at row i and column j. The performance of the ephemeris is gauged by the RSR, which ranges between $1/n$ and 1. Notably, a higher RSR indicates better performance of the ephemeris compared to DE436.

Table 5 displays the RSR of parameter deviations across eight pulsars with different ephemerides. It should be noted that the final column serves as comprehensive indicators. These are derived by summing the RSR of the eight pulsars based on a weight ratio, utilizing a weighting factor of the reciprocal of the pulsar rms value (Rodin & Fedorova 2022).

Figure 7 shows the effectiveness of various ephemerides in pulsar timing compared to DE436. The green dotted lines divide the picture into three parts. The ephemeris situated at the top position provides better support for pulsar timing, while the ephemeris positioned in the middle maintains a comparable level of performance. In contrast, those at the bottom are not recommended.

As affirmed in Table 5 and Figure 7, there are significant differences in DE200, DE405, INPOP06B, INPOP06C, and INPOP08A. The comprehensive evaluation indicators

Table 4
The Parameters of PSR J0437−4715 with Different Ephemerides

Ephemeris	RAJ/hms 04:37:15.81	DEC/dms −47:15:08	F0 s^{-1} 173.68794	F1 s^{-2} −1.728	PMRA mas yr^{-1}	PMDEC mas yr^{-1}
DE405	47711(29)	0.62405(4)	6184748(4)	281E−15	121.42565(36)	−71.48415(86)
DE414	46972(29)	0.62234(5)	6184744(4)	273E−15	121.42210(37)	−71.48465(87)
DE418	47111(29)	0.62247(9)	6184745(4)	268E−15	121.42125(42)	−71.48524(93)
DE421	47072(29)	0.62240(5)	6184746(4)	269E−15	121.42086(37)	−71.48521(87)
DE430	47383(29)	0.62254(7)	6184746(4)	270E−15	121.42409(39)	−71.48444(09)
DE435	47357(29)	0.62246(8)	6184747(4)	275E−15	121.42385(41)	−71.48466(92)
DE436	47357(30)	0.62246(0)	6184747(4)	274E−15	121.42389(44)	−71.48444(95)
DE438	47397(30)	0.62243(4)	6184748(5)	278E−15	121.42528(48)	−71.48404(01)
DE440	47352(30)	0.62244(2)	6184739(5)	275E−15	121.42217(46)	−71.48551(97)
EPM2011	47637(29)	0.62260(6)	6184736(4)	270E−15	121.42246(38)	−71.48437(89)
EPM2015	47550(29)	0.62267(6)	6184738(4)	271E−15	121.42344(39)	−71.48432(89)
EPM2017	47559(29)	0.62267(8)	6184738(4)	271E−15	121.42499(41)	−71.48380(91)
EPM2021	47423(29)	0.62250(8)	6184737(4)	271E−15	121.42241(41)	−71.48437(92)
INPOP06B	47074(29)	0.62184(7)	6184748(4)	279E−15	121.42851(39)	−71.48306(09)
INPOP06C	46964(29)	0.62234(7)	6184746(4)	274E−15	121.42412(39)	−71.48419(09)
INPOP08A	47044(28)	0.62224(5)	6184747(3)	270E−15	121.40789(24)	−71.49072(73)
INPOP10A	47277(30)	0.62230(5)	6184746(5)	273E−15	121.42947(05)	−71.48233(16)
INPOP13C	47125(29)	0.62251(3)	6184748(3)	279E−15	121.42771(34)	−71.48248(84)
INPOP17A	47393(29)	0.62268(5)	6184746(4)	272E−15	121.42517(37)	−71.48357(87)
INPOP19A	47493(29)	0.62261(6)	6184739(4)	275E−15	121.41582(39)	−71.48727(89)
INPOP21A	47565(29)	0.62281(7)	6184737(4)	276E−15	121.42025(39)	−71.48568(09)

Table 5
The RSR of Parameter Deviations of Eight Pulsars with Different Ephemerides

Ephemeris	J0437 −4715	J0613 −0200	J0711 −6830	J1022 +1001	J1024 −0719	J1744 −1134	J1939 +2134	J2145 −0750	SUM
DE405	0.381	0.298	0.361	0.405	0.429	0.302	0.448	0.480	0.686
DE414	0.560	0.647	0.540	0.571	0.377	0.556	0.599	0.480	1.049
DE418	0.500	0.528	0.647	0.575	0.496	0.556	0.579	0.460	0.994
DE421	0.492	0.583	0.663	0.611	0.579	0.639	0.456	0.583	1.054
DE430	0.786	0.655	0.607	0.754	0.841	0.738	0.671	0.734	1.423
DE435	0.905	0.917	0.742	0.853	0.905	0.865	0.909	0.937	1.677
DE438	0.679	0.671	0.734	0.821	0.770	0.750	0.734	0.702	1.336
DE440	0.659	0.766	0.671	0.476	0.782	0.663	0.651	0.659	1.262
EPM2011	0.496	0.444	0.452	0.429	0.393	0.468	0.536	0.452	0.907
EPM2015	0.595	0.429	0.444	0.524	0.528	0.468	0.484	0.587	1.025
EPM2017	0.524	0.500	0.421	0.373	0.472	0.484	0.357	0.488	0.949
EPM2021	0.635	0.591	0.472	0.500	0.548	0.655	0.663	0.611	1.182
INPOP06B	0.317	0.405	0.405	0.369	0.421	0.317	0.480	0.365	0.630
INPOP06C	0.369	0.440	0.476	0.433	0.468	0.389	0.437	0.389	0.736
INPOP08A	0.341	0.302	0.210	0.413	0.294	0.325	0.190	0.294	0.611
INPOP10A	0.540	0.421	0.357	0.341	0.464	0.603	0.405	0.452	1.006
INPOP13C	0.437	0.532	0.639	0.540	0.563	0.496	0.504	0.460	0.901
INPOP17A	0.635	0.690	0.758	0.730	0.722	0.754	0.794	0.694	1.297
INPOP19A	0.440	0.571	0.579	0.627	0.493	0.433	0.464	0.464	0.965
INPOP21A	0.663	0.563	0.710	0.496	0.508	0.484	0.591	0.659	1.158

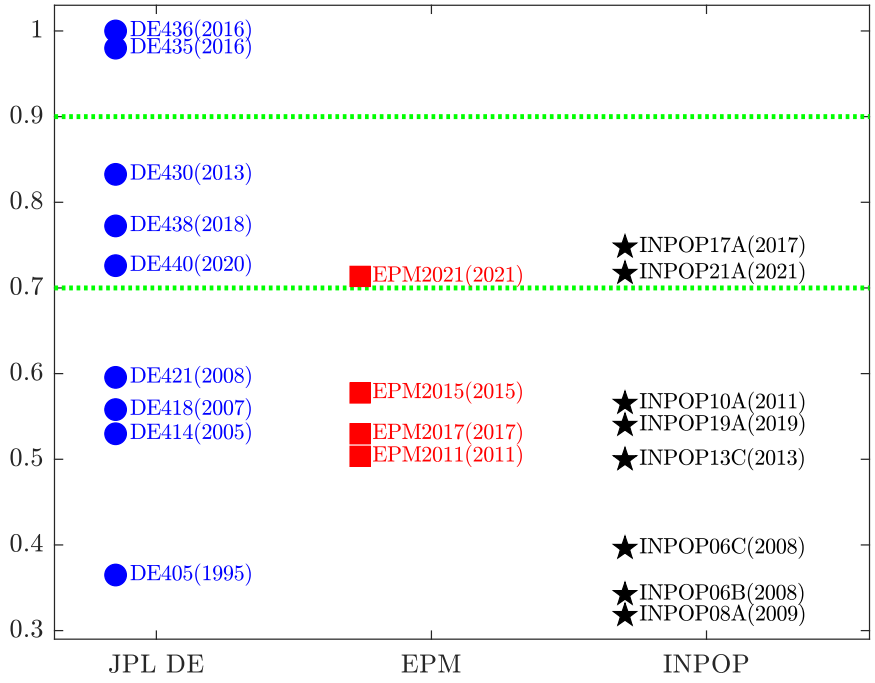

Figure 7. The performance of different ephemerides in pulsar timing. Three types of ephemerides are represented by different symbols, and the ordinate is the normalized comprehensive index.

of several ephemerides, including DE430, DE435, DE436, DE438, and INPOP17A, are relatively close. The recently released DE440, EPM2021, and INPOP21A show differences compared with previous ephemerides.

5. Summary

In this paper, we follow the steps of pulsar timing and analyze the differences in the Earth's position across different ephemerides. We also examine the discrepancies in correction terms and residuals. We focus on the parameters of the pulsar, conducting a comprehensive analysis of the performance of ephemeris in pulsar timing. However, a more in-depth understanding of the relationship between ephemeris and pulsar timing is still required. This may include exploring the impact of ephemeris errors on gravitational wave detection, as well as the dependence of the pulsar timescale on ephemeris. Discussion of these issues will improve our understanding between pulsar timing and ephemeris, thereby advancing related research. Considering the continuity and consistency of pulsar timing, it is necessary to pay attention to the differences caused by ephemeris in the future.

Acknowledgments

This work was funded by the Chinese Academy of Sciences (CAS) "Light of West China"Program, the Tianshan talents program (2023TSYCTD0013); The National Natural Science Foundation of China (NSFC, grant No. 12288102); The Major Science and Technology Program of Xinjiang Uygur Autonomous Region (No. 2022A03013-3).

Appendix
The Key Information About Some Ephemerides

The JPL DE, INPOP, and EPM series are the most accurate and widely used ephemeris, representing the highest level of human knowledge in the field of Solar system planetary ephemerides. The Table A1 displays key information of the main versions of ephemerides.

Table A1
A Brief List of Notable Update Events in Some Ephemerides

Ver (Rel) Span	Important update information
DE200 (1981) 1599-2201	It incorporates all available observational data from the period, serving as a cornerstone for the preparation of the U.S. Almanac spanning 1984 to 2003.
DE405 (1995) 1899-2050	It was included in the IERS in 2003, with an accuracy of 1 mas, and is frequently employed for calculating visual positions of celestial bodies (Pitjeva 2001).
DE414 (2005) 1899-2051	It has added space exploration data from the Mars Odyssey (ODY) probe in 2001, as well as the Mars Global Surveyor (MGS) in 2003.
DE418 (2007) 1899-2053	Its reference frame has been precisely aligned with ICRF using multiple VLBI measurements, achieving an accuracy of 0.25 mas (Folkner 2011).
DE421 (2008) 1550-2650	Through the calculation of asteroid perturbations on the inner planetary orbits, the accuracy of the lunar orbit reached the sub-meter level.
DE430 (2013) 1549-2650	It achieved an alignment accuracy of 0.2 mas to ICRF2, and the Mercury orbit was enhanced through the MESSENGER probe (Rhodes et al. 2019).
DE435 (2016) 1549-2650	The high-precision data with long time spans provided by the Cassini and New Horizons were used, which improved the accuracy of the Saturnian orbit.
DE436 (2016) 1549-2650	Various types of observation data have been further integrated, and the orbital precision has improved for all the planets (Baturin 2018).
DE438 (2018) 1549-2650	The important updates have been made to the Saturn orbit, and the Jupiter orbit was updated to support the Juno Navigation Group tasks.
DE440 (2020) 1550-2440	The addition of approximately 30 KBOs has notably enhanced the precision of Jupiter and Saturn's orbit calculations (Park et al. 2021).
DE441 (2020) BC13200-17191	It is used to analyze data beyond the time coverage of DE440, slightly sacrificing some short-term accuracy, but greatly increasing the time span (Park et al. 2021).
EPM2011 (2011) 1787-2214	It used data from the ODY, MRO, Cassini, ExoMars, and MEX, and served as the foundational basis for the Russian Astronomical Almanac (Pitjeva 2010).
EPM2015 (2015) 1787-2214	It used a total of 120,000 data points from different types of observations, and about 300 parameters have been determined (Narizhnaya et al. 2018).
EPM2017 (2017) 1787-2214	It used a total of over 800,000 data points from different types of observations, and a more efficient model was used (Pitjeva & Pitjev 2018).
EPM2021 (2021) 1787-2214	It has considered the tidal delay of the Moon, improved the parameters of the Sun and the Earth-Moon, and improved the KBO mass estimates (Pitjeva et al. 2022).
INPOP06B (2008) 1000-3000	It used around 45,000 observations including MEX, VEX, ODY, and MGS, and took account of the perturbation effects of more than 300 asteroids (Fienga et al. 2006).
INPOP06C (2008) 1000-3000	It used the same fitting data set as INPOP06B, but has improved modeling of asteroid-induced orbital perturbations (Fienga et al. 2006).
INPOP08A (2009) 1000-3000	It could provide positions, velocities, and rotation angles for the planets, as well as performed the conversion between TT and TDB (Fienga et al. 2009).
INPOP10A (2011) 1000-3000	There have been some changes in the dynamic modeling of the ephemeris, including the fitting process, data sets, and fitting parameters (Fienga et al. 2011).
INPOP13C (2013) 1000-3000	It reconfirmed the parameterized post-Newtonian (PPN) parameters that can be used to test Einstein's general theory of relativity.
INPOP17A (2017) 1000-3000	The asteroid orbits were fitted based on nearly 2 million observations obtained from the Gaia mission.
INPOP19A (2019) 1000-3000	It has used the data of Juno, Cassini, MEX, MESSENGER, and Gaia DR2, updated planetary masses, and changed some model algorithms. (Bernus et al. 2019)
INPOP21A (2021) 1000-3000	It utilized roughly 1.55 billion observations, and a new Bayesian procedure was used to calculate the masses of 343 main-belt asteroids (Fienga et al. 2022).

References

Ao, X., & He, A. 2020, JPhCS, 1616, 012072
Baturin, A. P. 2018, Sol. Syst. Res., 52, 355
Bernus, L., Minazzoli, O., Fienga, A., et al. 2019, PhRvL, 123, 161103
Caballero, R. N. 2018, in IAU Symp. 337, Pulsar Astrophysics the Next Fifty Years, ed. P. Weltevrede et al. (Cambridge: Cambridge Univ. Press), 154
Caballero, R. N., Guo, Y. J., Lee, K. J., et al. 2018, MNRAS, 481, 5501
Champion, D. J., Hobbs, G. B., Manchester, R. N., et al. 2011, in AIP Conf. Proc. 1357, Radio Pulsars: An Astrophysical Key to Unlock the Secrets of the Universe, ed. M. Burgay et al. (Melville, NY: AIP), 93
Deng, X. M., Fan, M., & Xie, Y. 2013, AcASn, 54, 550
Deng, Y. T., & Jin, S. G. 2022, Univ, 8, 360
Edwards, R. T., Hobbs, G. B., & Manchester, R. N. 2006, MNRAS, 372, 1549
Fienga, A., Bernus, L., Minazzoli, O., et al. 2022, arXiv:2211.04881
Fienga, A., Laskar, J., Kuchynka, P., et al. 2009, in Proc. Journées 2008 "Systèmes de référence spatio-temporels" & X. Lohrmann-Kolloquium: Astrometry, Geodynamics and Astronomical Reference Systems, ed. M. Soffel & N. Capitaine (Paris: Lohrmann-Observatorium and Observatoire de Paris), 65
Fienga, A., Laskar, J., Kuchynka, P., et al. 2011, CeMDA, 111, 363

Fienga, A., Manche, H., Laskar, J., & Gastineau, M. 2006, in 26th Meet. IAU, Precession and New Models in Fundamental Astronomy, Joint Discussion 16, 15
Folkner, W. M. 2011, in Proc. Journées 2010 "Systèmes de référence spatio-temporels" (JSR2010): New Challenges for Reference Systems and Numerical Standards in Astronomy, ed. N. Capitaine (Paris: Observatoire de Paris), 43
Folkner, W. M., Williams, J. G., Boggs, D. H., Park, R. S., & Kuchynka, P. 2014, Interplanetary Network Progress Report, 1, 42
Gui, M., Yang, H., Ning, X., et al. 2023, AdSpR, 71, 2669
Guo, Y. J., Li, G. Y., Lee, K. J., & Caballero, R. N. 2019, MNRAS, 489, 5573
Han, W., Wang, N., Wang, J. B., Yuan, J. P., & He, D. L. 2019, Ap&SS, 364, 48
Hilton, J. L., & Hohenkerk, C. Y. 2011, in Proc. Journées 2010 "Systèmes de référence spatio-temporels" (JSR2010): New Challenges for Reference Systems and Numerical Standards in Astronomy, ed. N. Capitaine (Paris: Observatoire de Paris), 77
Hobbs, G. 2012, arXiv:1205.6273
Hobbs, G. 2015, HiA, 16, 207
Hobbs, G., Edwards, R. T., & Manchester, R. N. 2006, MNRAS, 369, 655
Hobbs, G., Guo, L., Caballero, R. N., et al. 2020, MNRAS, 491, 5951
Irwin, A. W., & Fukushima, T. 1999, A&A, 348, 642
Jiang, N., Liu, J.-c., Zhu, Z., & Liu, N. 2023, PrA, 41, 198
Lazio, T. J. W., Bhaskaran, S., Cutler, C., et al. 2018, in IAU Symp. 337, Pulsar Astrophysics the Next Fifty Years, ed. P. Weltevrede et al. (Cambridge: Cambridge Univ. Press), 150
Lehman, D. H., Hoffman, T. L., & Havens, G. G. 2013, in Proc. 2013 IEEE Aerospace Conference (Piscataway, NJ: IEEE), 53
Li, L., Guo, L., & Wang, G.-L. 2016, RAA, 16, 58
Liu, N. 2021, AcASn, 62, 70
Liu, N., Zhu, Z., Antoniadis, J., Liu, J. C., & Zhang, H. 2023, A&A, 674, A187
Liu, W. Y., Zou, X. C., & Zhong, L. P. 2022, J. Geodesy Geodynamics, 042
Narizhnaya, N. V., Khovrichev, M. Y., Apetyan, A. A., et al. 2018, Sol. Syst. Res., 52, 312
Park, R. S., Folkner, W. M., Williams, J. G., & Boggs, D. H. 2021, AJ, 161, 105
Pitjeva, E. V. 2001, A&A, 371, 760
Pitjeva, E. V. 2006, in 26th Meet. IAU, Precession and New Models in Fundamental Astronomy, Joint Discussion 16, 14
Pitjeva, E. V. 2009, in Proc. Journées 2008 "Systèmes de référence spatio-temporels" & X. Lohrmann-Kolloquium: Astrometry, Geodynamics and Astronomical Reference Systems, ed. M. Soffel & N. Capitaine (Paris: Lohrmann-Observatorium and Observatoire de Paris), 57
Pitjeva, E. V. 2010, in IAU Symp. 261, Relativity in Fundamental Astronomy: Dynamics, Reference Frames, and Data Analysis, ed. S. A. Klioner, P. K. Seidelmann, & M. H. Soffel (Cambridge: Cambridge Univ. Press), 170
Pitjeva, E. V., Pavlov, D., Aksim, D., & Kan, M. 2022, in IAU Symp. 364, Multi-Scale (Time and Mass) Dynamics of Space Objects, ed. A. Celletti et al. (Cambridge: Cambridge Univ. Press), 220
Pitjeva, E. V., & Pitjev, N. P. 2018, AstL, 44, 554
Rhodes, B., van Kerkwijk, M., Davies, J., Eichhorn, H., & Rodríguez, J. 2019, JPLephem: Jet Propulsion Lab ephemerides package, Astrophysics Source Code Library, record, ascl:1908.017
Ridolfi, A., Gautam, T., Freire, P. C. C., et al. 2021, MNRAS, 504, 1407
Rodin, A. E., & Fedorova, V. A. 2022, AstL, 48, 321
Sun, S. B., Yang, Y. Z., Ma, Z. X., & Yan, J. G. 2022, J. Geomatics, 47, 5
Vallisneri, M., Taylor, S. R., Simon, J., et al. 2020, ApJ, 893, 112
Viswanathan, V., Fienga, A., Minazzoli, O., et al. 2018, MNRAS, 476, 1877
Wang, N., Xu, Q., Ma, J., et al. 2023, SCPMA, 66, 289512
Yao, J., Liu, J. C., Liu, N., et al. 2022, A&A, 665, A121